Multimedia Tools and Applications (2024) 83:46201–46220
https://doi.org/10.1007/s11042-023-17430-2

Automatic liver tumor detection and classification using the hyper tangent fuzzy C-Means and improved fuzzy SVM

Usharani Bhimavarapu[1]

Received: 7 February 2023 / Revised: 28 September 2023 / Accepted: 3 October 2023 /
Published online: 24 October 2023

Abstract
Globally liver diseases are the most life-threatening diseases, and according to global cancer statistics, liver cancer is the most common. Early detection of liver cancer can prevent millions of patients' mortality every year. Automatic liver cancer detection will help radiologists to determine the tumour identification and its severity, and it is also helpful to reduce the occurrence of errors which results in a reduction in the number of deaths from liver cancer. It gives more accurate results in less time, saving the radiologist's effort and time. The proposed model focused on improving the segmenting of liver images and then classifying the liver tumours from the CT images. The present study suggests the hyper tangent Fuzzy C-Means (HTFCM) to segment the liver images. It used Hyper tangent distance to calculate the data point distance from the cluster centres and obtained segmentation results almost closer to the ground truth liver images. Due to the fuzziness in the liver images, all state-of-the-art models except the proposed model cannot precisely locate the tumours. This study solved the issue of linear mapping using fuzzy logic, improved the classification accuracy, and reduced the processing time of early diagnosis of liver diseases. The proposed model improves the classification accuracy to 99.58% and reduces the processing time by 2-25 s to classify the liver tumours.

Keywords Image Processing · Liver Tumor · Unsupervised clustering · Hyper tangent

1 Introduction

It is believed that liver cancer forms in liver tissues and spreads there from other body parts [1]. When liver cancer is not detected promptly, it can cause severe complications and even death. Over 700,000 people die each year from liver cancer [2]. As a result, it is the leading cause of cancer death worldwide, and males have twice as high a risk as females [3, 4]. Radiologists and oncologists detect liver abnormalities with computed tomography (CT) and magnetic resonance imaging (MRI) [5]. The capture process of

✉ Usharani Bhimavarapu
ushafdp1122@gmail.com

[1] Department of Computer Science and Engineering, Koneru Lakshmaiah Education Foundation, Vaddeswaram, India

electronic devices produces distorted unclear objects, non-uniform intensity, and vague boundaries in CT scans or MRI images [6].

Tissues surround liver tumours; it is difficult for radiologists to determine their location. Performing a manual liver tumour diagnosis is time-consuming and inaccurate, delaying diagnosis and efficiency. The method is error-prone when it comes to classifying liver tumours. Noise, blurriness, and vague boundaries are common characteristics of medical images. There is inaccuracy and uncertainty in the edges of the different tumours in the liver image and in the descriptions of the tumours.

Using computer-assisted diagnosis (CAD) improves the accuracy of the characterization of liver tumours and lesions [1]. CAD systems help physicians diagnose liver lesions automatically, but it is difficult to identify their exact size. Applying soft computing and fuzzy logic could provide more clarity on tumours [7]. Soft computing techniques have been proposed for the extraction of liver features in some studies. Particle swarm optimization was applied to classify liver lesion features based on a bidirectional empirical mode decomposition [8]. Using edge-enhancing diffusion filtering and intensity-based registration, another study used anisotropic filtering followed by adaptive thresholding to segment tumours [9].

It used a region of interest (ROI)-based histogram for segmentation and a grey-level co-occurrence matrix to classify liver tumours to extract features from the liver images [10]. In [11], authors proposed an improved support vector machine (SVM) algorithm to cope with the underfitting and overfitting problems, but they encountered problems with linear mapping. The linear mapping of the score vector causes the SVM classifier to exaggerate data fitting issues. Fuzzy SVM calculates the feature scores for the ROI parts, which helps get better classification results and efficiently differentiate tumours.

The liver lesions are diagnosed into three categories such as meningioma, hepatocellular carcinoma, and metastatic carcinoma. To segment liver tumours, unsupervised machine learning-derived metastatic unsupervised segmentation is used [12]. Using SVM-based ANOVA and Modified Extreme Learning (MEL), liver cancers were classified, and region segmentation was used to segment liver CT abdomen images [13, 14]. There is more uncertainty in type 2 fuzzy set-based FCM when compared to type 1 fuzzy set-driven FCM [15]. A variant of FCM is proposed to eliminate noise, and the term credibility is introduced [16]. Using the entropy and hesitation degree of the membership function, an intuitionistic fuzzy set theory was presented [17].

It is susceptible to noise and results from incorrect segmentation, which makes fuzzy clustering with C-Means (FCM) ideal for many clustering problems [18]. FCM algorithms use Euclidian distance for finding the distance between data points and cluster centres, but the Euclidian distance can only detect spherical clusters. This study compared liver images with those in existing studies based on fuzzy logic. Fuzzy entropy was applied to map the original liver image, then its characteristics were considered. We enhanced the liver image using local information by extracting textual and edge information later.

Hyper tangent FCM (HTFCM) was proposed as an improved version of FCM; it computes data point distance from cluster canters using hyper tangent distance, enhancing the quality of liver image diagnosis with fuzzy segmentation. We reduced the noise in liver images by improving the Type 2 fuzzy concept. After hyper tangent segmentation has been applied, liver images are segmented using hyper tangents. Features are extracted to distinguish the tumours, and FSVM is used to classify the tumours.

1.1 Research contribution

The main contribution of the present study is:

1. In this study, we considered the LiTS, CHAOS and custom tumour dataset for liver tumours classification
2. To detect liver cancer in the CT scan liver image, we applied state-of-the-art segmentation models such as FCM, KPCM, IFCM and PFCM. We propose a hyper tangent FCM model and compare the proposed with the state-of-the-art segmentation models.
3. We applied the intensity and the textual feature extraction techniques
4. The experimental results are compared with the baseline classification models like SVM and Random Forest. We compared the proposed with the state-of-the-art classification models using the accuracy, sensitivity, and specificity classification performance metrics.
5. The proposed model surpassed the state-of-the-art models by 2–12% accuracy and processing time by 2-25 ms.

We organized the rest of the paper as follows. Section 2 goes with the material collection and the novelty followed in this research. Section 3 describes the experimental results, analyses the proposed improved optimization model behavior, and presents the results. Section 4 discusses the antecedents of diabetic retinopathy and their limits and overcome that limitation in the present research. Section 5 concludes the paper.

2 Materials and methodology

2.1 Materials

We collected 1200 CT images from LiTS [19], 3DIRCADb-1 (https://www.ircad.fr/research/data-sets/liver-segmentation-3d-ircadb-01/), CHAOS (https://explore.openaire.eu/search/dataset?pid=10.5281%2fzenodo.3362845), custom dataset. The collected dataset consists of all stages of liver cancer: 200 normal images, meningioma hepatocellular 300, and 300 metastatic CT images. We split the dataset as 80% for training and 20% for testing. The distribution of the collected dataset with CT categorical classification can be found in Table 1.

Table 1 Dataset distribution for this study

Category	Count	Training	Testing
Normal	200	160	40
Meningioma	400	320	80
hepatocellular	300	240	60
metastatic	300	240	60

Fig. 1 Block diagram of the proposed research

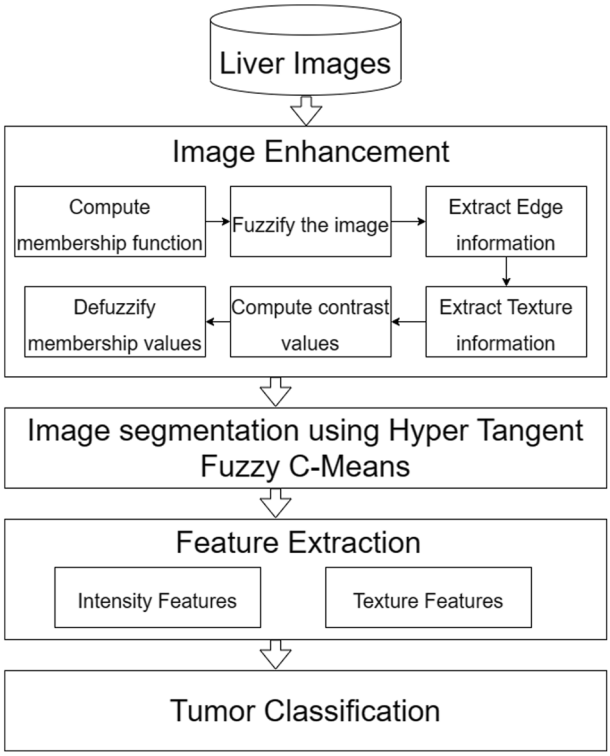

Fig. 2 Flow diagram of the proposed study

2.2 Methodology

The main objective of this study is to classify liver lesions into meningioma, hepatocellular carcinoma, and metastatic carcinoma. The proposed study is organized into four stages: Image preprocessing, segmentation, feature extraction and classification. Figure 1 shows the block diagram of the proposed study.

The noise and outliers in the liver images are removed, and the contrast of the liver image is improved in the image preprocessing stage. Next, the liver and the lesion regions are segmented. Later from the segmented liver images, features are extracted from the liver and the tumour. Finally, based on the extracted feature differences, the tumours are classified using the classifier. Figure 2 shows the flow of the present research,

2.2.1 Image enhancement

First, we converted all the liver images to grey-level images. Then the image enhancement is categorized as image normalization, image fuzzification, edge information and textual extraction. Figure 3 shows the difference between before performing the image processing and after image preprocessing.

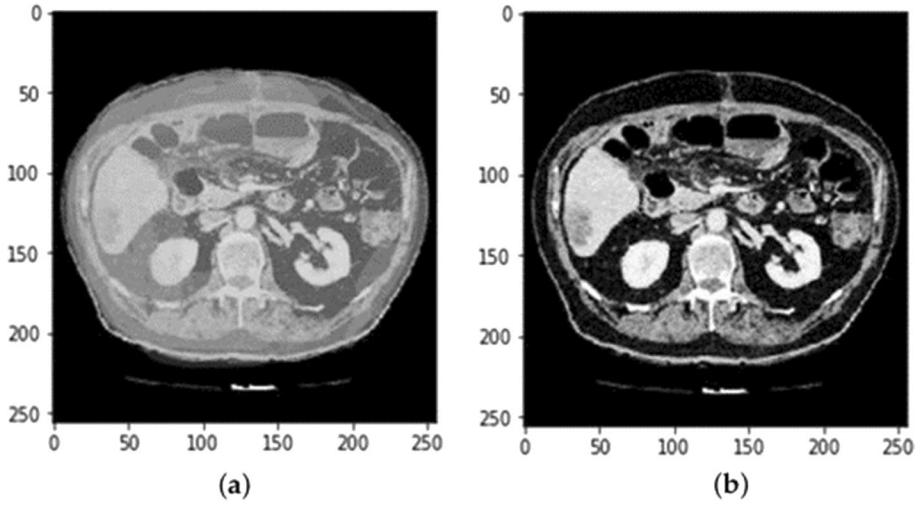

Fig. 3 (**a**) Before preprocessing (**b**) After preprocessing

Image normalization The range of the intensities in the liver image vary largely. So, we normalize the liver images by mapping the image intensity levels into the range $[O_{min,}O_{max}]$

$$\mathrm{O}(x,y) = O_{min} + \frac{\left(O_{max} - O_{min}\right) * (O_g(x,y) - O_{gmin})}{O_{gmax} - O_{gmin}} \tag{1}$$

where $O_{min} = 0 and O_{max} = 255. O_{gmax}$ and O_{gmin} are the maximum and the minimum intensity levels of the original liver image. $O_{max} and O_{min}$ are the maximum and the minimum intensity levels of the normalized liver image.O (i,j) and $(O_g(i,j)$ are the liver image levels of pixels(x,y) after and the before the normalization.

Image fuzzification We applied the S-membership function [20] to the gray level liver images which maps all the elements of into the real numbers in [0,1].

$$\mathrm{S}(r : \mathrm{i}, j, m) = \begin{cases} 0; r \le i \\ \frac{(g-i)}{(j-i)(m-i)}; i \le r \le j \\ 1 - \frac{(r-m)}{(m-j)(m-i)}; j \le r \le m \\ 1; r \ge m \end{cases} \tag{2}$$

The values in the above specified membership function represent the brightness of the pixel intensities of the liver image.

In liver images, the tissues and the tumors belong to the foreground and the all the remaining are considered as the background. From Eq. (2), the middle point j is determined as the image background classification [21] using the entropy [22]

Let B_x be the gray level probability distribution $x, x = 1, 2 \ldots \mathrm{N}. T_b$ is the below the threshold h,T_a is the above the threshold with maximum intensity N of the liver image. The output distribution is determined using the entropy and it is mathematically represented as:

$$T_b(h) = -\sum_{x=1}^{b} \frac{b_x}{B_b} ln \frac{b_x}{B_b} \tag{3}$$

$$T_a(h) = -\sum_{x=a+1}^{N} \frac{b_x}{1-B_b} ln \frac{b_x}{1-B_b} \tag{4}$$

$$\text{where } B_b = \sum_{x=1}^{b} b_x \tag{5}$$

The entropy is represented as

$$h^* = Ar\ gmax_{x=1}^{N} \left\{ B_a(t) + B_b(t) \right\} \tag{6}$$

Here h^* is the S member function middle point optimal threshold. Later we converted the image into the fuzzy domain using the S member function

$$\beta(x, y) = \mathrm{S}(\mathrm{O}(x, y) : i, h^*, m) \tag{7}$$

$$g_h(p) = \sum_{\substack{p=0 \\ 0 \le x \le B-1}}^{\substack{0 \le y <\le B-1 \\ \max(O(x,y))}} \delta(O(x, y) - p) \tag{8}$$

$$\delta(h) = \begin{cases} 0; h = 0 \\ 1; otherwise \end{cases} \tag{9}$$

where $O(x, y)$ pixel intensity for pixel (x, y), $g_h(p)$ is the liver gray image histogram, p is the gray level.

Edge normalization We applied the edge operator to the fuzzified liver image to extract the edge features of the liver images. The mathematical form of the edge operator is:

$$d_\beta(x, y) = \frac{\delta_\beta(x, y) - \delta_{\beta min}}{\delta_{\beta max} - \delta_{\beta min}} \tag{10}$$

where $\delta_{\beta min}$=min$(\delta_\beta(x, y))$ and $\delta_{\beta max}$= max$(\delta_\beta(x, y))$ $0 \le x \le height - 1$, $0 \le y \le width - 1$, width and height are the liver images width and height.$\delta_\beta(x, y)$ computed using the sobel operator [23].

Masking We applied four masks to determine the region of interest to highlight the edge and spot features. For this we used three vectors A=(1,3,5,3,1) B=(-1,0,2,0,-1) C=(-1,-2,0,2,1)

$$A^T B = \begin{bmatrix} 1 & 0 & 2 & 0 & -1 \\ -3 & 0 & 6 & 0 & -3 \\ -5 & 0 & 10 & 0 & -5 \\ -3 & 0 & 6 & 0 & -3 \\ -1 & 0 & 2 & 0 & -1 \end{bmatrix} \tag{M1}$$

$$A^T C = \begin{bmatrix} 1 & -2 & 0 & 2 & 1 \\ -3 & -6 & 0 & 6 & 3 \\ -5 & -10 & 0 & 10 & 5 \\ -3 & -6 & 0 & 6 & 3 \\ -1 & -2 & 0 & 2 & 1 \end{bmatrix} \tag{M2}$$

$$B^T A = \begin{bmatrix} 1 & -3 & -5 & -3 & -1 \\ 0 & 0 & 0 & 0 & 0 \\ 2 & 6 & 10 & 6 & 2 \\ 0 & 0 & 0 & 0 & 0 \\ -1 & -3 & -5 & -3 & -1 \end{bmatrix} \tag{M3}$$

$$C^T A = \begin{bmatrix} -1 & -3 & -5 & -3 & -1 \\ -2 & -6 & -10 & -6 & -2 \\ 0 & 0 & 0 & 0 & 0 \\ 2 & 6 & 10 & 6 & 2 \\ 1 & 3 & 5 & 3 & 1 \end{bmatrix} \tag{M4}$$

$$f_\beta(x,y) = \frac{abs\left(f_{\beta A^\top B}(p,q)\right)}{f_{\beta A^\top B_{max}}} * \frac{abs\left(f_{\beta A^\top C}(p,q)\right)}{f_{\beta A^\top C_{max}}} * \frac{abs\left(f_{\beta B^\top A}(p,q)\right)}{f_{\beta B^\top A_{max}}} * \frac{abs\left(f_{\beta C^\top A}(p,q)\right)}{f_{\beta C^\top A_{max}}} \tag{11}$$

where $f_{\beta A^\top B_{max}} = max(abs(f_{\beta A^\top B}(p,q)))$ and $f_{\beta A^\top C_{\max}} = \max(f_{\beta A^\top C_{\max}})$ and $f_{\beta B^\top A_{\max}} = \max(abs(f_{\beta B^\top A}(p,q)))$ and $f_{\beta C^\top A_{\max}} = \max(f_{\beta C^\top A_{\max}})\ 0 \le q \le height - 1, 0 \le p \le width - 1$

Contrast enhancement We measured the local mean of the texture and edge extraction in the fuzzy domain to improve the contrast of the image

$$C_\beta(x,y) = \frac{\left|\beta(x,y) - \overline{\beta}_d(x,y)\right|}{\left|\beta(x,y) + \overline{\beta}_d(x,y)\right|}; \tag{12}$$

$$\overline{\beta}_h(x,y) = \frac{\sum_{p=x-\frac{(h-1)}{2}}^{x+\frac{(h-1)}{2}} \sum_{q=y-\frac{(h-1)}{2}}^{y+\frac{(h-1)}{2}} \beta(p,q) * f_\beta(p,q) * d_\beta(p,q)}{\sum_{p=x-\frac{(h-1)}{2}}^{x+\frac{(h-1)}{2}} \sum_{q=y-\frac{(h-1)}{2}}^{y+\frac{(h-1)}{2}} f_\beta(p,q) * d_\beta(p,q)}; \tag{13}$$

where $\overline{\beta}_d(x,y)$ is the window local mean centered at location (x,y) with size h X h.

Defuzzification The enhanced pixel intensity can be obtained by the inverse function S^{-1} $(\beta\prime(x,y){:}i,j,m)$

$$
\begin{aligned}
O'(x,y) &= S^{-1}(\beta'(x,y) : \mathrm{i}, j, m) \\
&= O_{min} + \tfrac{O_{max}-O_{min}}{m-i}\sqrt{\beta'(i,j) * (j-i)(m-i)}; 0 \le \beta'(i,j) \le \tfrac{j-i}{m-i} \\
&= O_{min} + \tfrac{O_{max}-O_{min}}{m-i}(m-i-\sqrt{1-\beta'(i,j) * (m-j)(m-i)}; \tfrac{j-i}{m-i} \le \beta'(i,j) \le 1
\end{aligned} \tag{14}
$$

2.2.2 Tumor segmentation

HTFCM is the alternative solution to the limitations of the FCM.HTFCM clusters the data based on the hyperbolic distance between the data points and the cluster centres. Next, it allocates the membership values to the data points and these points are assigned to the clusters that are the highest membership degree. The mathematical form of the HTFCM is

$$
\begin{aligned}
g(x) &= \textstyle\sum_{p=1}^{m}\sum_{q=1}^{k}\beta_{pq}^{n}\delta_{c_{pq}^2}; \\
&= \textstyle\sum_{p=1}^{m}\sum_{q=1}^{k}\beta_{pq}^{n}\|\delta(a_q) - \delta(b_p)\|^2; \\
&= \textstyle\sum_{p=1}^{m}\sum_{q=1}^{k}\beta_{pq}^{n}\|1 - K(a_q, b_p)\|^2;
\end{aligned} \tag{15}
$$

$$
\text{Where } K(a_q, b_p) = 1 - tanh\left(-\frac{\| a_q - b_p \|^2}{\sigma^2}\right) \tag{16}
$$

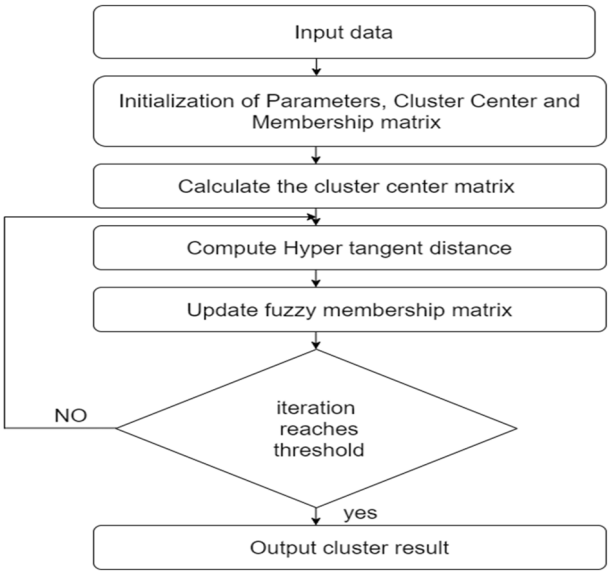

Fig. 4 Flow chart for the proposed segmentation

$$\beta_{pq} = \frac{1}{\sum_{p=1}^{m} \left(\frac{\delta_{C_{pm}^2}}{\delta_{C_{pm}^2}} \right) \frac{1}{n-1}} \tag{17}$$

$$\text{and } b_q = \frac{\sum_{q=1}^{k} \beta_p^n \cdot a_p}{\sum_{q=1}^{k} \beta_p^n} \tag{18}$$

and a_q is the data point.

Algorithm 1 gives the details about the proposed HTFCM, and Fig. 4 shows its flow diagram.

1.Initial cluster centres set the number of cluster, fuzzy index and the maximum number of iterations

2. for each iteration

update matrix using eq(15)

update cluster center suing hyper tangent

3. Output results

Algorithm 1 Proposed HTFCM

2.2.3 Feature extraction

The feature extraction phase characterizes the lesion in the liver images. For liver images, the tissues surround the tumour region, and to signify the difference, we use the intensity and texture features. Intensity features are mean, standard deviation, skewness, and kurtosis and the Texture features are wavelet and Gabor energy.

2.2.4 Intensity features

(a) *Mean*

$$\text{Mean(E)} = \frac{1}{M} \sum_{(pq) \in R} T(p, q); \tag{19}$$

where M is the total no: of pixels in the liver image, T is the total no: of pixels in region of interest (p,q) are the pixel gray level at position p and q.

(b) *Standard deviation*

$$\text{S} = \sqrt{\frac{\sum_{(pq) \in R} (T(p, q) - E)^2}{M}}; \tag{20}$$

E is the mean of the liver image.

(c) *Kurtosis*

$$\text{Kurtosis} = \frac{1}{M}\frac{\sum_{(pq)\in ROI}(T(p,q)-E)^4}{S^4} \tag{21}$$

(d) *Skewness*

$$\text{Skewness(N)} = \frac{1}{M}\frac{\sum_{(pq)\in ROI}(T(p,q)-E)^3}{S^3} \tag{22}$$

2.2.5 Tumor classification

The extracted features are the input to the fuzzy SVM [24] to classify the liver tumour images. We categorized the tumours into meningioma, hepatocellular carcinoma, and metastatic carcinoma. The fuzzy SVM uses feature vectors to calculate the feature score for ROI, which helps in classifying the tumours.

For a classification set with fuzzy membership function $F=\{(p_1,q_1,\beta_1),\ldots.(p_i,q_i,\beta_i,),\ldots\ldots.(p_n,q_n,\beta_n)\}$ where $p_i \epsilon \mathbb{R}^n$ and $q_i \in Q$,$Q=\{+1,-1\}$,β_i is the membership function for the sample p_i belonging to q_i and $0 \le \beta_i \le 1$ and the hyperplane is defined as $T^W \cdot \phi(p) + a = 0$ to separate the samples and maximize the margin.

The mathematical representation of the FVSM classifier is

$$g(p) = S\left|\sum_{j=1}^{m} q_i \beta_i^* K(p_i.p) + a^*\right|; \tag{23}$$

where $a^* and \beta_i^*$ and represents the bias and the Lanrange multiplier and $\beta_i^*>0$ is the support vector.

For multi class classifier one against other(OAO) [23] is defined in this study. For a set of n classes,$(p_i, q_i, \beta_i,)$, i=1,2,…..$p_i \epsilon \mathbb{R}^n$ and $q_i \in Q$,$Q=\{+1,-1\}$.

The steps for OAO procedure are:

1. One class is taken as the positive class and the remining (n-1) classes are considered as negative class.
2. Construct a binary FSVM classifier and name it as FSVM1;
3. Exclude the first class and turn to (n-1) class for classification and later construct FSVM classifier for the remaining (n-1) classes
4. (n-1) FSVMs has been constructed for n class classification

For each training sample calculate the fuzzy membership based on the distance between it and classification hyperplane and cluster center.

$$\beta_i = \begin{cases} 1 - \frac{c(p_i)}{m+\delta}; c(p_i) \le C \\ \left(1 - \frac{C}{m+\delta}\right).\left(\frac{1}{1+c(p_i)-C}\right); c(p_i) > C \end{cases} \tag{24}$$

where β_i represents the fuzzy membership for the sample p_i. $c(p_i)$ is the distance between the sample p_i and the cluster center p_0 and it is represented as $\|p_i - p_0\|$. M represents the radius of the sample cluster and it is represented as $\max\|p_i - p_0\|$ where p_0 is the

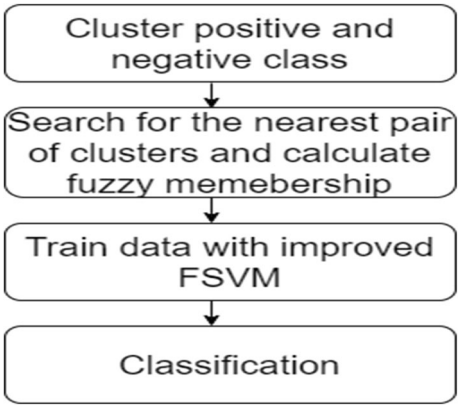

Fig. 5 Flow chart for IFSVM

hyperplane and p_i locates on the same side ofp_0. δ=0.1 and C is the distance between the hyperplane and the cluster center.

Algorithm 2 gives the details about the improved algorithm used for the classification in this research and the Fig. 5 shows the flowchart for the flow of that algorithm.

1.Initial fuzzy membership function,hyperplane and the maximum number of iterations

2. for each iteration

- One class is taken as the positive class and the remining (n-1) classes are considered as negative class.
- Construct a binary FSVM classifier and name it as FSVM1;
- Exclude the first class and turn to (n-1) class for classification and later construct FSVM classifier for the remaining (n-1) classes
- (n-1) FSVMs has been constructed for n class classification

3. For each training sample update cluster center using eq(24)

4. Output results

Algorithm 2 Proposed FSVM

3 Experimental results

All the experiments are implemented using python on a computer with configuration Intel core i7@2.00 GHz, 8 GB RAM. A model was built for testing the conventional fivefold cross validation was taken into account.

3.1 Evaluation metrics

$$\text{DICE} = \frac{2 * |TP|}{|TP| + |FN| + |FP|} \tag{25}$$

$$\text{Rand Index} = \frac{\textit{Correct similar pairs} + \textit{correct dissimilar pairs}}{\textit{Total number of pairs}} \tag{26}$$

$$\text{Hausdroff distance} = \max\left(\underset{p \in P}{max}\ \underset{q \in Q}{min} \lVert p - q \rVert_2, \underset{q \in Q}{max}\ \underset{p \in P}{min} \lVert p - q \rVert_2\right) \tag{27}$$

$$\text{Accuracy} = \frac{|TP| + |TN|}{|TP| + |FN| + |TN| + |FP|} \tag{28}$$

$$\text{Precision} = \frac{|TP|}{|TP| + |FP|} \tag{29}$$

$$\text{Recall} = \frac{|TN|}{|TN| + |FP|} \tag{30}$$

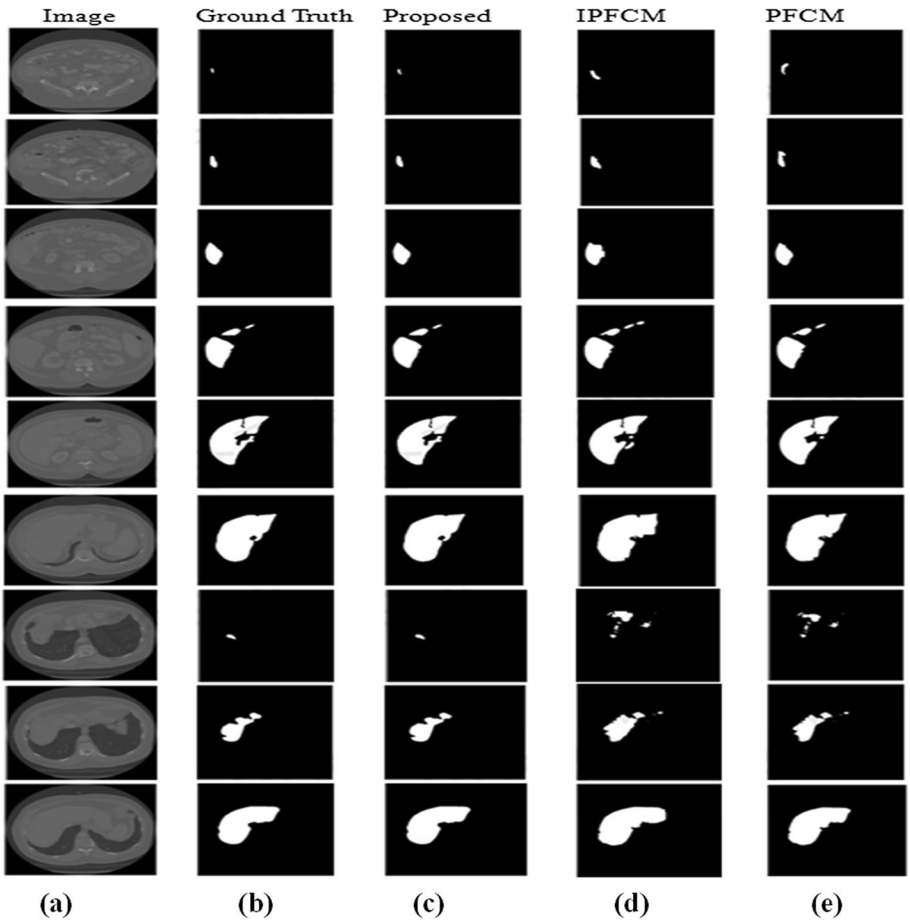

Fig. 6 Comparison of segmented ROI of proposed with the state-of-the-art models for Custom dataset (**a**) Original Image (**b**) Ground truth (**c**) Proposed (**d**) IPFCM (**e**) PFCM

$$\text{F1} - \text{score} = \frac{2 * Precision * Recall}{|Precision| + |Recall|} \tag{31}$$

3.2 Liver tumor segmentation evaluation

Due to the vagueness of the medical images, all the state-of-the-art models except the proposed model cannot detect blood clots. Figure 6 compares the segmented region of interest proposed with the state-of-the-art models. The proposed model rejects the unwanted tissues and areas and detects the tumour regions only. Figure 4 shows that the proposed model could obtain the segmentation results almost closer to the ground truth. Figure 6 shows that the PFCM model does not precisely recognize the tumour region. After comparing all model results with the ground truths, we identified that the proposed model almost accurately detects the exact shape and size of the tumour region. The proposed model surpasses every state-of-the-art model in that the remaining models detect the tumour regions in the liver image. However, the size and shape of the tumour are not accurate compared to the ground truth.

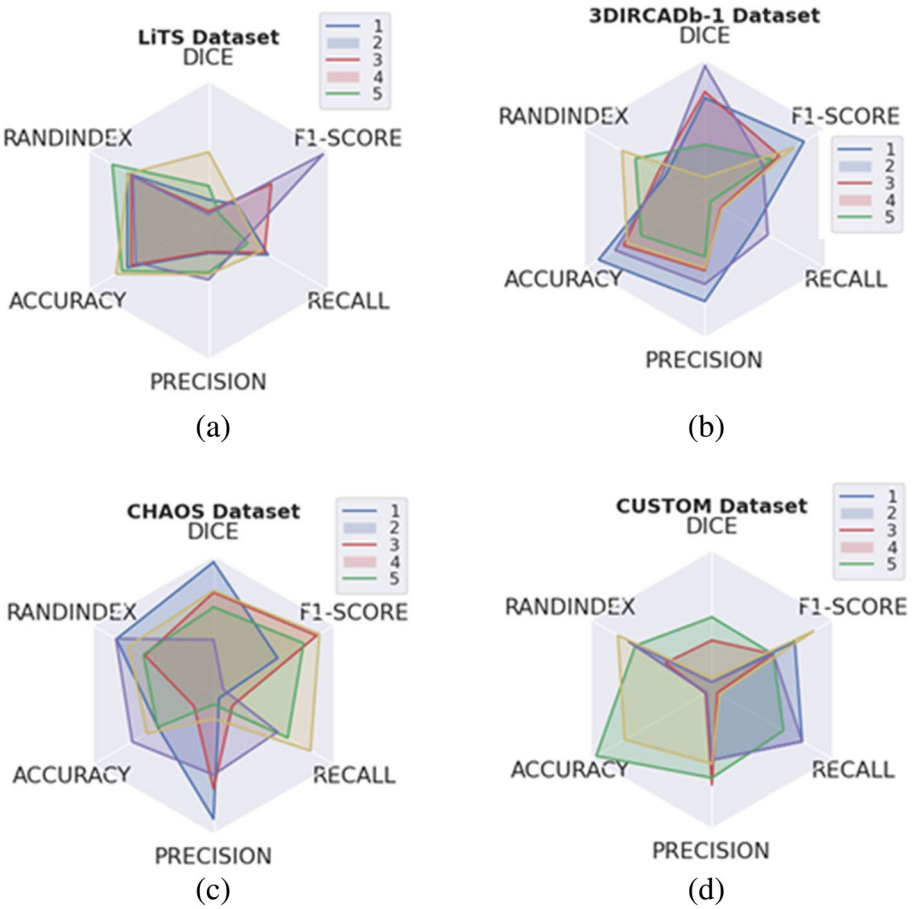

Fig. 7 Segmentation analysis of the dataset (**a**) 3DIRCADb01 (**b**) LiTS (**c**) CHAOS (**d**) custom

Figure 7 represents the performance analysis of the proposed segmentation results for the dataset 3DIRCADb01, LiTS, CHAOS, custom. We evaluated the different experiments by considering various measures, including Dice, rand index accuracy, precision, recall and accuracy. We also assessed the five experimental results.

We compared the segmented region of interest proposed with the state-of-the-art models and tabulated the results in Table 2. We compared the segmentation results of liver tumours proposed with the otsu, FCM, IFCM, PFCM, IPFCM, HDensenet, and K-Means. Table 2 tabulated the accuracy and the processing time of the state-of-the-art models. For 3DIRCADb01, the proposed obtained an accuracy of 99.18%, followed by Resnet with an accuracy of 99.02%, then Otsu with an accuracy of 98.51% and IPFCM with an accuracy of 97.84%. The processing time for the proposed segment of the liver image is 8 s, followed by Resnet and IPFCM at 9 s and PFCM at 10 s. The accuracy of the proposed model surpasses other existing state-of-the-art models by 2–10% and reduces the processing time by 2-14 s.

3.3 Liver tumor classification evaluation

The tumour's crucial features are tested and trained by FSVM. All the features are extracted from the collected region of interest. Later the feature selection process is carried out to optimize the feature set. Finally, the optimized features are used to train and test the FSVM. Figure 8 shows the confusion matrix for performing the multiclass classification of liver diseases.

After the segmentation of the liver tumour region, features are extracted separately. The classifier classifies the liver tumour from the obtained features into meningioma, hepatocellular carcinoma, and metastatic carcinoma. We compared the proposed classification performance with the state-of-the-art models and tabulated the results in Table 3. The classification accuracy obtained by the state of the art models(Random forest, Randomized tree, J48, KNN, SVM, Naïve Bayes) are 90.74%, 94.71%, 95.47%, 91.43%, 96.48%, 91.84%.The proposed HTFCM with FSVM achieved the uppermost classification accuracy. The proposed model achieved precision and Recall of 98.36% and 1.00%.

Table 2 Comparison of accuracy and processing time of segmented image of the proposed with state of the art models

Algorithm used	3DIRCADb01		LiTS		CHAOS		Custom	
	A(%)	P(s)	A(%)	P(s)	A(%)	P(s)	A(%)	P(s)
Otsu [25]	98.51	11	97.86	15	97.67	17	98.74	15
FCM [26]	93.66	22	95.75	22	93.37	22	93.74	26
IntuitionistFCM [27]	94.68	11	94.87	11	95.68	11	94.58	11
Possibilistic FCM [28]	95.36	10	95.58	10	96.73	10	95.68	10
Intuitionist Possibilistic FCM [29]	97.84	9	96.48	9	96.58	10	97.79	15
HDensenet [30]	90.46	13	91.57	14	91.58	11	90.58	13
Stacked encoder [31]	96.47	11	95.73	11	94.64	11	96.29	15
Resnet [32]	99.02	9	98.58	9	98.69	12	99.22	13
En-Dnet [33]	97.86	12	96. 85	12	98.58	12	97.39	12
HTFCM	**99.18**	**8**	**98.69**	**8**	**98.80**	**9**	**99.01**	**10**

A Accuracy, *P* Processing Time

Fig. 8 Confusion matrix

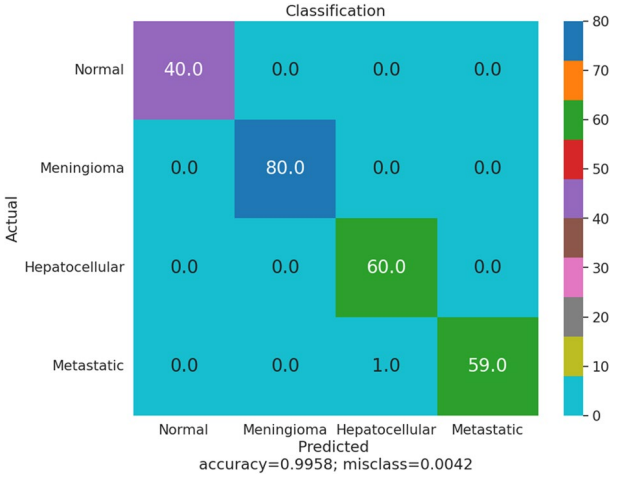

The requirement for training and the testing time of various algorithms are tabulated in Table 4. From the results, we observed that the proposed model has less movement and testing time for input liver images.

The analysis is carried out on various k-fold cross-validations. Table 5 tabulates the values of the study of the proposed model with the state-of-the-art models by considering different cross-validations. The table tabulates the other splits of the training and testing sets with cross-validation analysis. The results show that the proposed achieved an accuracy of 98.73% for a 70-30 split, 99.58% for an 80-20 division and 99.29% for a 90-10 split. This reveals that the split plays a vital role in classification accuracy.

4 Discussion

The study aimed to detect liver cancer and classify tumours using CT scans. Early lung cancer indicators include enlarged and widened nodules, the primary visual features radiologists observe. When lung cancer is in its early stages, the inside structure and the borders of the lungs appear very subtle. As a result, diagnosis becomes very challenging, and identifying abnormal and normal regions becomes difficult.

A hyper tangent FCM was proposed to segment the liver images to detect the tumour region from a CT scan liver tumour. This study first processed the noise in the liver images

Table 3 Classification comparison of proposed with state of the art models

s.no	Model	Accuracy(%)	Precision(%)	Recall(%)	F1-score(%)
1	Randomforest [34]	90.74	75.46	89.46	78.83
2	Randomized tree [35]	94.71	77.94	92.54	77.95
3	WGDL + GMM + DNN [11]	99.38	97.33	99.78	98.14
4	HFCNN [36]	97.22	78.48	92.98	78.27
5	CascadedCNN [37]	94.21	91.43	97.38	84.73
6	DeeplapV3 [38]	98.50	89.45	93.56	79.78
7	Proposed	**99.58**	**98.36**	**1.00**	**99.17**

Table 4 Training and Testing analysis

Model	Training time(s)	Testing time(s)
Random forest [34]	2536	34.53
Randomized tree [35]	2364	28.46
WGDL + GMM + DNN [11]	2242	18.43
HFCNN [36]	2168	16.64
CascadedCNN [37]	2142	13.64
DeeplapV3 [38]	2124	11.45
Proposed	2015	9.47

Table 5 Cross validation analysis

Model	70–30 split	80-20split	90-10split	Cross validation
[39]	86.77	93.83	95.85	96.36
[40]	88.76	95.46	97.43	95.85
[41]	90.53	95.73	98.57	93.75
[42]	90.51	96.84	99.28	94.73
Proposed	**98.73**	**99.58**	**99.29**	**98.63**

using fuzzy image preprocessing and converted the liver images to a fuzzy set. The processed image is segmented using the proposed hyper tangent FCM to detect the tumours in the liver images. The proposed model ceases the effect of outliers during the clustering process. The proposed HTFCM is evaluated and compared its performance with state-of-the-art FCM models. This analysis proves that the proposed model surpassed the other state-of-the-art models. Finally, classified the extracted features and compared the classification accuracy with the state-of-the-art models.

Liver image enhancement is critical for radiologists and CAD systems. By using fuzzy logic and liver image characteristics, we implemented image enhancement. We identified tumour features scattered throughout the liver image using edge and texture information and mapped them to maximum fuzzy entropy. When the FCM considers membership categories category-wise, data points are abnormal. A traditional clustering method cannot handle noise and outliers in medical images. We used hyper tangent clustering to segment medical images. Unfortunately, the image could not be extracted in its entirety.

FSVM performance was compared with classical SVM, and all features were used for the classifiers in these experiments. In FSVM, every training image is assigned a membership, which weakens the influence of noise and outliers on classification accuracy. In the current input features and data, the fuzzy theory improves the classification performance of SVM better than classical SVM.

Standard FCM does not eliminate the noise and outliers in the medical images. A hyper tangent FCM enables the recognition of outliers, minimises the outliers' effect, and ceases it. It further detects and extracts the outliers in the medical image segmentation. The proposed framework delivered excellent results very quickly and efficiently. It can also be tried with tumours other than liver tumours, as the hyper tangent FCM showed promising results.

Chlebus et al. [34] classified DR using Random forest and achieved accuracy of 90.74%, sensitivity of 75.46%, specificity of 89.46%, F1-score of 78.83%. Jansen et al. [35] used the Randomized tree and achieved accuracy of 94.71%, sensitivity of 77.94%, specificity of 92.54%, F1-score of 77.95%. Das et al. [11] proposed a hybrid model

WGDL+ GMM+DNN and achieved accuracy of 99.38%, sensitivity of 77.33%, specificity of 92.78%, F1-score of 78.14%. Dong et al. [36] proposed a novel model HFCNN and achieved accuracy of 97.22%, sensitivity of 78.48%, specificity of 92.98%, F1-score of 78.27%. Soler et al. [37] developed a CascadedCNN model and achieved accuracy of 94.21%, sensitivity of 91.43%, specificity of 97.38%, F1-score of 84.73%. Othman et al. [38] proposed a novel DeeplapV3 model and achieved accuracy of 99.50%, sensitivity of 89.45%, specificity of 93.56%, F1-score of 79.78%.

The proposed framework correctly detects most parts of the tumour with an accuracy of 99.18% for tumour segmentation and 98.58% for tumour classification. But still, some false positives could be improved by applying false positive filters on a large dataset. The framework could be improved to handle all types of datasets and will make more widely accepted by hospitals or other institutes. In addition, we considered a limited dataset, and future research should be carried out to increase the dataset size.

5 Conclusion

This study proposed a hyper tangent FCM to segment the liver images to detect the tumour region from a CT scan liver tumour. This study first processed the noise in the liver images using fuzzy image preprocessing and converted the liver images to a fuzzy set. The processed image is segmented using the proposed hyper tangent FCM to detect the tumours in the liver images. The proposed model ceases the effect of outliers during the clustering process. The proposed HTFCM is evaluated and compared its performance with state-of-the-art FCM models. This analysis proves that the proposed model surpassed the other state-of-the-art models. Finally, classified the extracted features and compared the classification accuracy with the state-of-the-art models.

The tumours exist in different shapes and sizes; we will try to plug a mechanism to incorporate the position and the channel feature information and capture more spatial information in the intra-slices and inter-slices of the 3D medical data. Due to the different layer thicknesses of the data, there is an individual difference in the abdominal features there is a need to solve the continuity of adjacent layers. It is necessary to standardize the imaging parameters and collect more data to establish training in future datasets to optimize further and improve the segmentation results. In future work, the segmentation and classification accuracy could be improved by introducing different research models for segmentation and classification.

Data availability Yes.

Declarations

Conflict of interest Authors do not have conflict of interest.

References

1. Deshmukh SP, Choudhari D, Amalraj S, Matte PN (2023) Hybrid deep learning method for detection of liver cancer. Comput Assist Methods Eng Sci 30(2):151–65. https://doi.org/10.24423/cames.463

2. ABOUT LIVER CANCER, https://www.Cancer.Org/Cancer/Liver-Cancer/. Accessed 20 Oct 2022
3. Almotairi S, Kareem G, Aouf M, Almutairi B, Salem MA (2020) Liver tumor segmentation in CT scans using modified segnet. Sensors 20(5):1516. https://doi.org/10.3390/s20051516
4. Siegel RL, Miller KD, Wagle NS, Jemal A (2023) Cancer statistics, 2023. Ca Cancer J Clin 73(1):17–48. https://doi.org/10.3322/Caac.21763
5. Christ PF, Elshaer ME, Ettlinger F, Tatavarty S, Bickel M, Bilic P, Rempfler M, Armbruster M, Hofmann F, D'Anastasi M, Sommer WH (2016) Automatic Liver And Lesion Segmentation In CT Using Cascaded Fully Convolutional Neural Networks And 3D Conditional Random Fields. In medical Image Computing And Computer-Assisted Intervention–MICCAI 2016: 19th International Conference, Athens, Greece, October 17–21, Proceedings, Part II 19 2016. Springer International Publishing, pp 415–423. https://doi.org/10.1007/978-3-319-46723-8_48
6. Lebre MA, Vacavant A, Grand-Brochier M, Rositi H, Abergel A, Chabrot P, Magnin B (2019) Automatic segmentation methods for liver and hepatic vessels from CT And MRI volumes, applied to the Couinaud scheme. Comput Biol Med 1(110):42–51. https://doi.org/10.1016/j.compbiomed.2019.04.014
7. Kozlov OV, Kondratenko YP, Skakodub OS (2023) Intelligent information technology for structural optimization of fuzzy control and decision-making systems. Inartificial Intelligence In Control And Decision-Making Systems: Dedicated To Professor Janusz Kacprzyk. Cham: Springer Nature Switzerland, pp 127–165. https://doi.org/10.1007/978-3-031-25759-9_7
8. Acharya UR, Koh JE, Hagiwara Y, Tan JH, Gertych A, Vijayananthan A, Yaakup NA, Abdullah BJ, Fabell MK, Yeong CH (2018) Automated diagnosis of focal liver lesions using bidirectional empirical mode decomposition features. Comput Biol Med 1(94):11–18. https://doi.org/10.1016/j.compbiomed.2017.12.024
9. Alirr OI, Rahni AA, Golkar E (2018) An automated liver tumour segmentation from abdominal CT scans for hepatic surgical planning. Int J Comput Assist Radiol Surg 13:1169–1176. https://doi.org/10.1007/s11548-018-1801-z
10. ShanmugaSundaram P, Santhiyakumari N (2019) An enhancement of computer aided approach for colon cancer detection in WCE images using ROI based color histogram and SVM2. J Med Syst 43(2):29. https://doi.org/10.1007/s10916-018-1153-9
11. Das A, Acharya UR, Panda SS, Sabut S (2019) Deep learning based liver cancer detection using watershed transform and Gaussian mixture model techniques. Cogn Syst Res 1(54):165–175. https://doi.org/10.1016/j.cogsys.2018.12.009
12. Kadoury S, Vorontsov E, Tang A (2015) Metastatic liver tumour segmentation from discriminant Grassmannian manifolds. Phys Med Biol 60(16):6459. https://doi.org/10.1088/0031-9155/60/16/6459
13. Kaya Y, Kuncan F (2022) A hybrid model for classification of medical data set based on factor analysis and extreme learning machine: FA+ ELM. Biomed Signal Process Control 1(78):104023. https://doi.org/10.1016/j.bspc.2022.104023
14. Devi RM, Seenivasagam V (2020) Automatic segmentation and classification of liver tumor from CT image using feature difference and SVM based classifier-soft computing technique. Soft Comput 24:18591–18598. https://doi.org/10.1007/s00500-020-05094-1
15. Zhou S, Li D, Zhang Z, Ping R (2020) A new membership scaling fuzzy C-Means clustering algorithm. IEEE Trans Fuzzy Syst 29(9):2810–2818. https://doi.org/10.1109/tfuzz.2020.3003441
16. Dhruv B, Mittal N, Modi M (2023) Hybrid particle swarm optimized and fuzzy C Means clustering based segmentation technique for investigation of COVID-19 infected chest CT. Comput Methods Biomech Biomed Eng: Imaging Vis 11(2):197–204. https://doi.org/10.1080/21681163.2022.2061376
17. Dahiya S, Gosain A (2023) A novel Type-II intuitionistic fuzzy clustering algorithm for mammograms segmentation. J Ambient Intell Human Comput 14(4):3793–3808. https://doi.org/10.1007/s12652-022-04022-5
18. Phamtoan D, Vovan T (2023) The fuzzy cluster analysis for interval value using genetic algorithm and its application in image recognition. Comput Stat 38(1):25–51. https://doi.org/10.1007/s00180-022-01215-6
19. Lits-Liver Tumor Segmentation Challenge, https://Competitions.Codalab.Org/Competitions/17094. Accessed 20 Oct 2022
20. Ejegwa PA, Onyeke IC, Kausar N, Kattel P (2023) A new partial correlation coefficient technique based on intuitionistic fuzzy information and its pattern recognition application. Int J Intell Syst 6:2023. https://doi.org/10.1155/2023/5540085
21. Ma P, Li C, Rahaman MM, Yao Y, Zhang J, Zou S, Zhao X, Grzegorzek M (2023) A state-of-the-art survey of object detection techniques in microorganism image analysis: from classical methods to deep learning approaches. Artif Intell Rev 56(2):1627–1698. https://doi.org/10.1007/s10462-022-10209-1

22. Mishra AP, Noida SI, Bajpai MM, Singhal MS, Tripathi MJ, Sinha MP, Bhardwaj P (2023) Adaptive non linear deblurring technique: a new image enhancement technique. Semicond Optoelectron 42(1):34–42. https://doi.org/10.1109/42.712133
23. Jähne B (1995) Concepts, algorithms, and scientific applications. Digit Image Processing 1(1):1–320
24. Lou C, Xie X (2023) Multi-view intuitionistic fuzzy support vector machines with insensitive pinball loss for classification of noisy data. Neurocomputing 14:126458. https://doi.org/10.1016/j.neucom.2023.12645
25. Yang P, Song W, Zhao X, Zheng R, Qingge L (2020) An improved Otsu threshold segmentation algorithm. Int J Comput Sci Eng 22(1):146–153. https://doi.org/10.1504/ijcse.2020.107266
26. Bo W, Ying W, Lijie C (2020) Fuzzy clustering recognition algorithm of medical image with multiresolution feature. Concurr Comput: Pract Exp 32(1):E4886. https://doi.org/10.1002/cpe.4886
27. Shynu PG, Shayan HM, Chowdhary CL (2020) A fuzzy based data perturbation technique for privacy preserved data mining. In 2020 International Conference On Emerging Trends In Information Technology And Engineering (Ic-ETITE). IEEE, pp 1–4. https://doi.org/10.1109/ic-etite47903.2020.244
28. Pal NR, Pal K, Keller JM, Bezdek JC (2005) A possibilistic fuzzy C-Means clustering algorithm. IEEE Trans Fuzzy Syst 13(4):517–530. https://doi.org/10.1109/tfuzz.2004.840099
29 Chowdhary CL, Mittal M, K P, Pattanaik PA, Marszalek Z (2020) An efficient segmentation and classification system in medical images using intuitionist possibilistic fuzzy C-Mean clustering and fuzzy SVM algorithm. Sensors 20(14):3903. https://doi.org/10.3390/s20143903
30. Ke Q, Zhang J, Wei W, Połap D, Woźniak M, Kośmider L, Damaševĭcius R (2019) A neuro-heuristic approach for recognition of lung diseases from X-Ray images. Expert Syst Appl 15(126):218–232. https://doi.org/10.1016/j.eswa.2019.01.060
31. Ahmad M, Qadri SF, Ashraf MU, Subhi K, Khan S, Zareen SS, Qadri S (2022) Efficient liver segmentation from computed tomography images using deep learning. Comput Intell Neurosci 18:2022. https://doi.org/10.1155/2022/2665283
32. Rahman H, Bukht TF, Imran A, Tariq J, Tu S, Alzahrani A (2022) A deep learning approach for liver and tumor segmentation in CT images using Resunet. Bioengineering 9(8):368. https://doi.org/10.3390/bioengineering9080368
33. Appadurai JP, Kavin BP, Lai WC (2023) En–Denet based segmentation and gradational modular network classification for liver cancer diagnosis. Biomedicines 11(5):1309. https://doi.org/10.3390/biomedicines11051309
34. Chlebus G, Meine H, Moltz JH, Schenk A (2017) Neural network-based automatic liver tumor segmentation with random forest-based candidate filtering. Arxiv Preprint Arxiv:1706.00842. https://doi.org/10.48550/arxiv.1706.00842
35. Jansen MJ, Kuijf HJ, Veldhuis WB, Wessels FJ, Viergever MA, Pluim JP (2019) Automatic classification of focal liver lesions based on MRI and risk factors. PLoS ONE 14(5):E0217053. https://doi.org/10.1371/journal.pone.0217053
36. Dong X, Zhou Y, Wang L, Peng J, Lou Y, Fan Y (2020) Liver cancer detection using hybridized fully convolutional neural network based on deep learning framework. IEEE Access 1(8):129889–129898. https://doi.org/10.1109/access.2020.3006362
37. Soler L, Hostettler A, Agnus V, Charnoz A, Fasquel JB, Moreau J, Osswald AB, Bouhadjar M, Marescaux J (2010) 3D image reconstruction for comparison of algorithm database. https://www.ircad.fr/research/data-sets/liver-segmentation-3d-ircadb-01. Accessed 20 Oct 2022
38. Othman E, Mahmoud M, Dhahri H, Abdulkader H, Mahmood A, Ibrahim M (2022) Automatic detection of liver cancer using hybrid pre-trained models. Sensors 22(14):5429. https://doi.org/10.3390/s22145429
39. Midya A, Chakraborty J, Srouji R, Narayan RR, Boerner T, Zheng J, Pak LM, Creasy JM, Escobar LA, Harrington KA, Gönen M (2023) Computerized diagnosis of liver tumors from CT scans using a deep neural network approach. IEEE J Biomed Health Inform. https://doi.org/10.1109/jbhi.2023.3248489
40. Amritha M, Manimegalai P (2023) Liver tumor segmentation and classification using deep learning. In 2023 Fifth International Conference On Electrical, Computer And Communication Technologies (ICECCT). IEEE, pp 01–07 https://doi.org/10.1109/icecct56650.2023.10179731
41. Vasundhara N, Nandan AS, Hemanth SV, Macherla S, Madhura GK (2023) An efficient biomedical solicitation in liver cancer classification by deep learning approach. In 2023 IEEE International Conference On Integrated Circuits And Communication Systems (ICICACS). IEEE, pp 01–05. https://doi.org/10.1109/icicacs57338.2023.10099828

42. Sowparnika B, Yamini K, Walid MA, Prasad J, Aparna N, Chauhan A (2023) Innovative Method For Detecting Liver Cancer Using Auto Encoder And Single Feed Forward Neural Network. In2023 2nd International Conference On Applied Artificial Intelligence And Computing (ICAAIC). IEEE, pp 156–161. https://doi.org/10.1109/icaaic56838.2023.10140207